Theory of pulse propagation and wave-mixing processes under intense resonant excitation

S. S. Montasser,* J. Miletic,† and B. Hönerlage
Institut de Physique et Chimie des Matériaux de Strasbourg, Groupe d'Optique Nonlinéaire et d'Optoélectronique, 5 rue de l'Université, F 67084 Strasbourg, France
(Received 6 April 1989)

We study the temporal and spatial evolution of a pump, test, and signal field generated in a four-wave-mixing process for resonant excitation of a nonlinear medium by nanosecond pulses. The propagation effects for the pulses are taken into account beyond the usual mean-field approximation. The model is then applied to a three-level system, describing CuCl at low temperatures. A great deal of new information concerning the temporal and spatial structures of the different fields propagating through the sample is obtained. We show, for instance, that the temporal shapes of the interacting fields are well established after propagation through the first few micrometers of the sample. Beyond this, they propagate with a diminishing amplitude. We also show that these structures are due to the dephasing of the fields throughout their propagation as well as to the temporal evolution of the absorption and generation function of the sample.

I. INTRODUCTION

Degenerate four-wave mixing has been shown to be a powerful technique to study optical transitions in semiconductors.[1,2] In this type of experiment, a pulsed laser beam is split into two parts, labeled pump and test beams. These beams are then focused under small angles into a slab of the material, having a thickness of a few micrometers. The nonlinear interaction gives rise to a nonlinear polarization which coherently generates a pulse of the same frequency, namely the signal pulse. These three pulses propagate through the sample. In this process, two photons are absorbed from the pump pulse and the generation of the signal pulse is induced by the test pulse.[3–8] It is a coherent process in which the virtual intermediate state decays, yielding one photon to the test beam and one to the signal beam without any collision process. Therefore, since no real quasiparticles are excited by the preceding two-photon absorption, the signal intensity is a function of the instantaneous fields of the exciting light beams (pump and test) only. The signal generation follows adiabatically the exciting fields. Based on the expansion of the polarization in terms of the electric light field, this nonlinear polarization is of third order. Since this perturbation expansion converges rapidly[1,2] off resonance, it is usually truncated in order to study nonlinear processes.

Closer to resonance and at high-field intensities, the perturbation treatment breaks down and the full dielectric susceptibility χ has to be considered.[9,10] In addition, a population of real quasiparticles is then created which influences the absorption, the dispersion, and the nonlinear optical properties of the material.[9,11] This is especially important under pulsed excitation conditions when the population dynamics governs the time evolution of the nonlinear susceptibility.[11–13] The influence of these populations was studied in Ref. 9, where the nonlinear susceptibility was calculated as a function of exciting fields, while, in Ref. 11, the time dependence of the amplitudes of these fields was taken into account, resulting in a memory effect, shown to be dependent on the lifetime of the populations. This memory effect has been observed near resonances in four-wave-mixing experiments performed on a nanosecond time scale.[13] In these experiments, structures in the temporal shape of the signal appear.[14] They have different origins: besides the memory effect of the complex nonlinear dielectric function, the generation of the signal rate varies between oscillatory attenuation and gain due to competition between coherent and incoherent scattering processes. The effect of this competition on the wave mixing and its application to the case of CuCl was studied,[15,16] and it was found that incoherent processes not only diminish the signal generation but also lead to temporal structures which depend on the lifetimes of the quasiparticles created during the excitation. In this study, the time dependence of the wave-mixing process is described in the mean-field approximation for the exciting pump pulse, neglecting propagation effects.

The propagation of a picosecond exciting pulse and its effect on the population of the quasiparticles was studied[17] by solving numerically the equation of evolution of the density-matrix elements together with Maxwell's equations, near the two-photon resonance. It was found that in this frequency range the pulse is strongly altered and the excitonic and biexcitonic levels show a population inversion.

To our knowledge, the competition between the part of the dielectric susceptibility, leading to a nonlinear absorption, and its coherent part, giving rise to an induced emission and a reconstitution of the propagating pulse, has not been extensively discussed in the literature. It is the aim of this work to perform a theoretical study of the degenerate four-wave-mixing processes in three-level systems, where the time dependence as well as the effect of the propagation of the exciting resonant fields and the generated signal field are taken into account. To do this, we cut the sample into slices of variable thickness Δz, the output fields of each slice being the input ones of the next. For each slice, the population and hence the sus-

ceptibility χ and the absorption coefficient α are then calculated in terms of the mean field of the incoming pump beam. The slice thickness is chosen so that $\alpha\Delta z \ll 1$ (we took $\alpha\Delta z \leq 0.04$). Inside each slice the population rate equations are integrated numerically (using Grear's method), while the variation of the fields is calculated analytically. At the front part of the sample, the field amplitudes are real but its imaginary parts start growing as the fields propagate through the sample. This can be considered as a dephasing of the propagating fields due to the dispersion and absorption in the sample.

In Sec. II we describe the model and the physics involved in this process and in Sec. III we discuss the result of the numerical calculation done in the case of CuCl modeled by a three-level system (ground state, excitonic, and biexcitonic levels), when wave mixing occurs and we excite at the biexciton resonance.

II. THEORY AND MODEL OF CALCULATION

A. Coherent and incoherent susceptibility

Let us consider as interacting fields an intense pump pulse (p) and a frequency degenerate test pulse (t). They both propagate almost collinearly in a nonlinear medium and generate the signal beam (s). If we neglect transverse effects—that is, take the medium and the fields as homogeneous in the x and y directions—and if we consider the propagation in the z direction only, the linearly polarized electric fields $E_i(z,t)$ (with $i=p,s,t$) can be described by plane waves:

$$E_i(z,t)=\tfrac{1}{2}[E_i^0(z,t)e^{i(\omega t-k_i z)} + E_i^{0*}(z,t)e^{-i(\omega t-k_i z)}] , \quad (1)$$

where all the complex field envelopes $E_i^0(z,t)$ are assumed to be slowly varying with respect to the rapid variation of $e^{i\omega t}$ and e^{ikz}. The nonlinear wave equation can then be written as

$$\frac{\partial^2}{\partial z^2}E_i(z,t)-\mu_0\sigma\frac{\partial}{\partial t}E_i(z,t)-\mu_0\frac{\partial^2}{\partial t^2}E_i(z,t) = \mu_0\frac{\partial^2}{\partial t^2}P_{\rm NL}^i(z,t) . \quad (2)$$

σ is the linear conductivity of the system and $P_{\rm NL}^i(z,t)$ the nonlinear polarization of the ith beam which, in turn, is related to the nonlinear susceptibility tensor $\chi_{\rm NL}^{ij}$ and to the jth electric field $E_j(z,t)$ via the convolution product

$$P_{\rm NL}^i(z,t)=\sum_j\int_{-\infty}^{t}\chi_{\rm NL}^{ij}(z,t,t')E_j(z,t')dt' , \quad (3)$$

if we assume local spatial response for simplicity. $\chi(z,t,t')$ can be separated into slowly and quickly varying terms in space (wave vector nk_n) and time (frequency $n\omega$) via the expansion

$$\chi_{\rm NL}^{ij}(z,t,t')=\sum_n\chi_{\rm NL}^{ij(n)}(z,t,t')e^{in(\omega t-k_n z)} . \quad (4)$$

If the field amplitudes $E_i^0(z,t)$ vary slowly in time with respect to $\chi_{\rm NL}^{ij(n)}(z,t,\tau)$, we may define time- and frequency-dependent susceptibility components[11] by

$$\chi_{\rm NL}^{ij(n)}(z,t,\omega)=\int_0^\infty\chi_{\rm NL}^{ij(n)}(z,t,\tau)e^{-i\omega\tau}d\tau . \quad (5)$$

Using (1), (3), and (5) together with the relation $\chi(z,t,\omega)=\chi^*(z,t,-\omega)$, we obtain for the nonlinear polarization component $P_{\rm NL}^i(z,t)$

$$P_{\rm NL}^i(z,t)=\frac{1}{2}\left[\sum_{j,n}\chi_{\rm NL}^{ij(n)}(z,t,\omega)E_j^0(z,t)e^{i[(n+1)\omega t-(nk+k_j)z]}+\chi_{\rm NL}^{ij(n)}(z,t,\omega)E_j^{0*}(z,t)e^{i[(n-1)\omega t-(nk-k_j)z]}\right] . \quad (6)$$

Keeping in (6) all terms which oscillate at frequency ω, we find

$$P_{\rm NL}^{i\omega}(z,t)=\frac{1}{2}\left[\sum_j\chi_{\rm NL}^{ij(0)}(z,t,\omega)E_j^0(z,t)e^{i(\omega t-k_j z)}+\chi_{\rm NL}^{ij(2)*}(z,t,\omega)E_j^{0*}(z,t)e^{i[\omega t-(2k_n-k_j)z]}\right] . \quad (7)$$

We can now solve Eq. (2) in the slowly varying envelope approximation by neglecting all time derivatives of the functions $E_j^0(z,t)$ and $\chi_{\rm NL}^{ij(n)}$. We can also neglect $(\partial^2/\partial z^2)E_j^0(z,t)$ with respect to $k_j(\partial/\partial z)E_j^0(z,t)$. Using the dispersion relation $\mu_0\epsilon_1\omega^2=k_i^2$ we obtain

$$\frac{\partial}{\partial z}E_i^0(z,t)=\frac{-\omega\mu_0\sigma E_i^0(z,t)}{2k_i}+\frac{\omega^2\mu_0}{2ik_i}\left[\sum_j E_j^0(z,t)e^{-i(k_j-k_i)z}+E_j^{0*}(z,t)e^{-i(2k_n-k_j-k_i)z}\right] . \quad (8)$$

If we restrict ourselves to the phase-matching condition $\Delta k=0=2k_p-k_t-k_s$ and assume that the test and signal beams are so weak that they do not introduce changes in the nonlinear susceptibility,[18] we get for the differential equations governing the propagation of the pump, test, and signal pulses (indices p,t,s)

$$\frac{\partial}{\partial z}E_p^0(z,t)=\frac{-\mu_0\omega\sigma}{2k_p}E_p^0(z,t)+\chi_{\rm NL}^{pp(0)}(z,t,\omega)\frac{\mu_0\omega^2}{2ik_p}E_p^0(z,t) + \chi_{\rm NL}^{pp(2)*}(z,t,\omega)\frac{\mu_0\omega^2}{2ik_p}E_p^{0*}(z,t) , \quad (9)$$

$$\frac{\partial}{\partial z}E_t^0(z,t)=\frac{-\mu_0\omega\sigma}{2k_t}E_t^0(z,t)+\chi_{\rm NL}^{tt(0)}(z,t,\omega)\frac{\mu_0\omega^2}{2ik_t}E_t^0(z,t)+\chi_{\rm NL}^{ts(2)*}(z,t,\omega)\frac{\mu_0\omega^2}{2ik_t}E_s^{0*}(z,t)\ , \tag{10}$$

$$\frac{\partial}{\partial z}E_s^0(z,t)=\frac{-\mu_0\omega\sigma}{2k_s}E_s^0(z,t)+\chi_{\rm NL}^{ss(0)}(z,t,\omega)\frac{\mu_0\omega^2}{2ik_s}E_s^0(z,t)+\chi_{\rm NL}^{st(2)*}\frac{\mu_0\omega^2}{2ik_s}E_t^{0*}(z,t)\ . \tag{11}$$

As discussed in Refs. 12 and 13, the first term on the right-hand side of Eqs. (9)–(11) gives rise to the linear absorption and the second one to the nonlinear absorption and dispersion induced by the pump beam. These terms do not distinguish between the coherence or incoherence of the excited states involved in the calculation of the susceptibility for the interacting beams. The last term, on the contrary, represents a parametric process in which the pump and test beams generate the signal beam coherently, i.e., only coherent states contribute to this generation [via $\chi_{\rm NL}^{st(2)*}(z,t)$].

Now let us write Eqs. (9)–(11) in the compact form

$$\frac{\partial E_i^0}{\partial z}=AE_i+BE_j^*\ , \tag{12}$$

where

$$A=\left[\frac{-\omega\mu_0\sigma}{2k}-\frac{\mu_0\omega^2}{2k}\mathrm{Im}\chi_{\rm NL}^{ii(0)}\right]+i\left[-\mathrm{Re}\chi_{\rm NL}^{ii(0)}\frac{\mu_0\omega^2}{2k}\right]\ , \tag{13}$$

$$B=\left[-\mathrm{Im}\chi_{\rm NL}^{ij(2)*}\frac{\mu_0\omega^2}{2k}\right]+i\left[-\mathrm{Re}\chi_{\rm NL}^{ij(2)*}\frac{\mu_0\omega^2}{2k}\right]\ .$$

If we solve Eqs. (12) for a slice of the sample with the incoming fields $E_i^{(1)}$ and $E_j^{(1)}$, the variation of the fields in the z direction inside the slice can be described by

$$E_i=e^{a_1 z}E_i^{(1)}\left[\cosh\lambda z+ia_2\frac{\sinh\lambda z}{\lambda}\right]+E_j^{(1)*}B\frac{\sinh\lambda z}{\lambda}\ , \tag{14}$$

where $\lambda^2=b_1^2+b_2^2-a_2^2$ is a parameter which we will call the "regeneration function" and a_1,a_2, and b_1,b_2 are the real and imaginary parts of A and B, respectively. In the case of $\lambda^2<0$, the hyperbolic functions are replaced by the corresponding trigonometric ones. In Eqs. (12)–(14) (i,j) are replaced by (p,p) for the pump beam, (t,s) for the test beam, and (s,t) for the signal beam.

The mean field inside the slice m of thickness Δz can be calculated from the relation

$$E_p^m=\frac{1}{\Delta z}\int_{z_m}^{z_m+\Delta z}E_p(z,t)dz\ . \tag{15}$$

Using Eq. (14), we obtain

$$E_p^m=\frac{a_1}{\Delta z(a_1^2-\lambda^2)}\left\{E_p^{(1)}\left[e^{a_1\Delta z}\left[\cosh\lambda\Delta z-\frac{\lambda^2}{a_1}\frac{\sinh\lambda\Delta z}{\lambda}\right]-1\right]+\left[E_p^{(1)*}B+iE_p^{(1)}a_2\right]\left[e^{a_1\Delta z}\left[\frac{\sinh\lambda\Delta z}{\lambda}-\frac{\cosh\lambda\Delta z}{a_1}\right]+\frac{1}{a_1}\right]\right\}\ . \tag{16}$$

The initial conditions for the first slice can be taken as $E_p^{(1)}=(I_p^0)^{1/2}$, $E_t^{(1)}=(I_t^0)^{1/2}$, and $E_s^{(1)}=0$, where the fields are real and I_p^0 and I_t^0 are the incident pump- and test-beam intensities, respectively. Equations (14) and (16) govern the propagation of the three interacting fields inside the sample. To use them we have to know the coherent and the incoherent parts of the susceptibility, which we will determine below.

B. Application to CuCl

In order to determine the coherent and incoherent parts of the susceptibility, we will consider a three-level system which is well adapted to describe CuCl. As discussed in more detail in Refs. 9, 11, and 19, it consists of the crystal ground state $|1\rangle$, the exciton state $|2\rangle$, and the biexciton state $|3\rangle$, having energies 0, $E_{\rm ex}$, and $E_{\rm bi}$, respectively. The transition between states $|1\rangle$ and $|2\rangle$ and $|3\rangle$ are dipole allowed for linear polarization, while those between $|1\rangle$ and $|3\rangle$ are allowed for two-photon transitions. The Hamiltonian H in the dipole approximation can be written as

$$H=H_0-\mu E\ , \tag{17}$$

where H is the Hamiltonian of the noninteracting system, μ is the dipole operator, and E is the exciting electric field (the field of the pump beam in our case).

In the framework of the density-matrix formalism, the polarization $P(z,t)$ can be expressed by[20]

$$P(z,t)=N\,\mathrm{tr}[\rho(z,t)\mu]\ , \tag{18}$$

where N is the density of the molecules in the crystal. The matrix representation of the dipole operator μ is

$$\mu=\begin{bmatrix}0&\mu_{\rm ex}&0\\ \mu_{\rm ex}&0&\mu_{\rm bi}\\ 0&\mu_{\rm bi}&0\end{bmatrix}\ , \tag{19}$$

where

$$\mu_{\rm ex}=\langle 2|\mu|1\rangle \tag{20a}$$

and

$$\mu_{\rm bi}=\langle 3|\mu|2\rangle\ . \tag{20b}$$

We can find from (18)–(20)

$$P(z,t)=N\{[\rho_{12}(z,t)+\rho_{21}(z,t)]\mu_{ex} + [\rho_{23}(z,t)+\rho_{32}(z,t)]\mu_{bi}\} . \quad (21)$$

We now develop the density-matrix elements $\rho_{ij}(z,t)$ into a series in order to separate quickly and slowly varying contributions,[21]

$$\rho_{ij}(z,t)=\sum_n \rho_{ij}^n(z,t)e^{in(\omega t-kz)} . \quad (22)$$

Inserting this expression into Eq. (21) and keeping only the terms which oscillate with the frequency ω, we get

$$P^\omega=P_L^\omega+P_{NL}^\omega = N\{[\rho_{12}^1(z,t)+\rho_{21}^1(z,t)]\mu_{ex} + [\rho_{23}^1(z,t)+\rho_{32}^1(z,t)]\mu_{bi}\}e^{i(\omega t-kz)} , \quad (23)$$

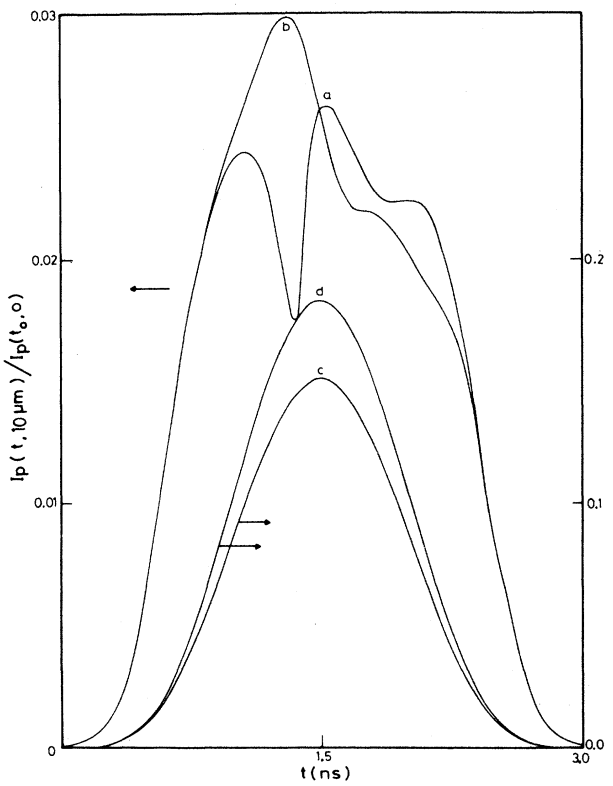

FIG. 1. Temporal shape of the initially Gaussian pump pulse after its propagation through a sample of CuCl of 10 μm thickness. The maximum intensity of the incident pulse is $n_p=5\times10^{14}$ photons/cm^3 and its photon energy $\hbar\omega=3.186$ eV. It is *a*, calculated from Eqs. (14) and (16); *b*, neglecting the induced recombination (that is, setting $\chi_{NL}^{(2)*}=0$); *c*, as in *a*, but taking the whole sample as one slice only (mean-field approximation); and *d*, as in *b*, but within the mean-field approximation.

where P_L^ω is the linear polarization which is given by

$$P_L^\omega=\chi_L E_p(z,t)e^{i(\omega t-kz)} . \quad (24)$$

P_{NL}^ω is given by Eq. (7) and χ_L denotes the linear susceptibility. Using Eq. (7), Eq. (23) can be written as

$$E_p(z,t)\chi^{(0)}(z,t)+E_p^*(z,t)\chi^{(2)*}(z,t) = E_p[\chi(z,t)-\chi_L]=E_p\chi_{NL}(z,t) , \quad (25)$$

where

$$\chi(z,t)=\frac{2N}{\epsilon_0 E_p(z,t)}\{[\rho_{12}^1(z,t)+\rho_{21}^1(z,t)]\mu_{ex} + [\rho_{23}^1(z,t)+\rho_{32}^1(z,t)]\mu_{bi}\} \quad (26)$$

gives the dielectric susceptibility and χ_{NL} its nonlinear part. We may now calculate the time dependence of ρ through the time-dependent Schrödinger equation, which leads to (20),

$$\frac{\partial\rho_{ij}(z,t)}{\partial t}=\frac{i}{\hbar}[\rho(z,t),H]_{ij}-\rho_{ij}(z,t)\Gamma_{ij} , \quad (27)$$

where H is the Hamiltonian of the system and Γ_{ij} denote the different damping constants which we will discuss later on. Using now expansion (22), and following the same procedure as in Ref. 11 but considering the propagation of the fields with complex amplitude, we get for the rate equations of $\rho_{ij}^n(z,t)$

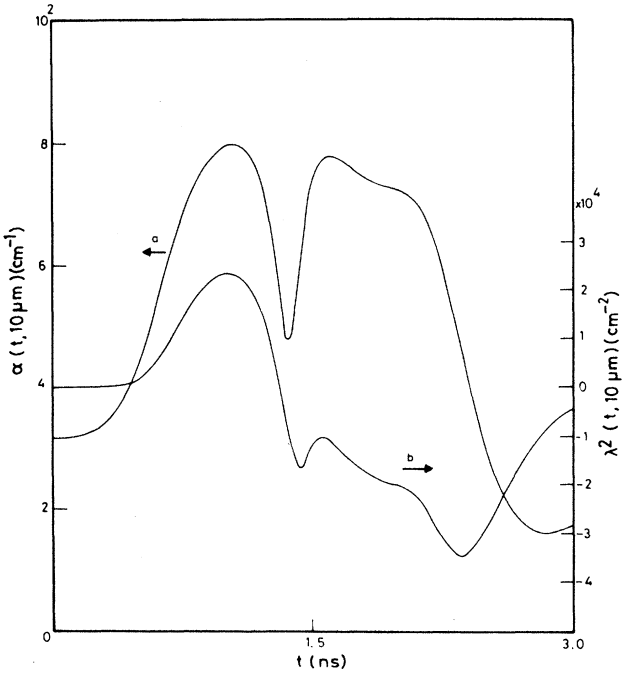

FIG. 2. Time dependence of the absorption coefficient α (curve *a*) and of the regeneration function λ^2 (curve *b*) at the end of the sample for the conditions of Fig. 1(a).

$$
\begin{aligned}
i\hbar\frac{\partial\rho_{12}^{n}(z,t)}{\partial t} &= -(E_{\mathrm{ex}}-n\hbar\omega+i\hbar\Gamma_{12})\rho_{12}^{n}(z,t)+\frac{\mu_{\mathrm{bi}}}{2}[E_p(z,t)\rho_{13}^{n-1}(z,t)+E_p^*(z,t)\rho_{13}^{n+1}(z,t)] \\
&\quad+\frac{\mu_{\mathrm{ex}}}{2}[E_p(z,t)(\rho_{11}-\rho_{22})^{n-1}(z,t)+E_p^*(z,t)(\rho_{11}-\rho_{22})^{n+1}(z,t)] , \\
i\hbar\frac{\partial\rho_{13}^{n}(z,t)}{\partial t} &= -(E_{bi}-n\hbar\omega+i\hbar\Gamma_{13})\rho_{13}^{n}(z,t)+\frac{\mu_{\mathrm{bi}}}{2}[E_p(z,t)\rho_{12}^{n-1}(z,t)+E_p^*(z,t)\rho_{12}^{n+1}(z,t)] \\
&\quad-\frac{\mu_{\mathrm{ex}}}{2}[E_p(z,t)\rho_{23}^{n-1}(z,t)+E_p^*(z,t)\rho_{23}^{n+1}(z,t)] , \\
i\hbar\frac{\partial\rho_{23}^{n}(z,t)}{\partial t} &= -(E_{\mathrm{bi}}-E_{\mathrm{ex}}-n\hbar\omega+i\hbar\Gamma_{23})\rho_{23}^{n}(z,t)-\frac{\mu_{\mathrm{ex}}}{2}[E_p(z,t)\rho_{13}^{n-1}(z,t)+E_p^*(z,t)\rho_{13}^{n+1}(z,t)] \\
&\quad+\frac{\mu_{\mathrm{bi}}}{2}[E_p(z,t)(\rho_{22}-\rho_{33})^{n-1}(z,t)+E_p^*(z,t)(\rho_{22}-\rho_{33})^{n+1}(z,t)] , \\
i\hbar\frac{\partial}{\partial t}(\rho_{11}-\rho_{22})^{n}(z,t) &= -i\hbar\Gamma_1\delta_{n,0}-(n\hbar\omega-i\hbar\Gamma_1)(\rho_{11}-\rho_{22})^{n}(z,t) \\
&\quad+\frac{\mu_{\mathrm{bi}}}{2}\{E_p(z,t)[\rho_{23}^{n-1}(z,t)-\rho_{32}^{n-1}(z,t)]+E_p^*(z,t)[\rho_{23}^{n+1}(z,t)-\rho_{32}^{n+1}(z,t)]\} \\
&\quad-\mu_{\mathrm{ex}}\{E_p(z,t)[\rho_{12}^{n-1}(z,t)-\rho_{21}^{n-1}(z,t)]+E_p^*(z,t)[\rho_{12}^{n+1}(z,t)-\rho_{21}^{n+1}(z,t)]\} , \\
i\hbar\frac{\partial}{\partial t}(\rho_{22}-\rho_{33})^{n}(z,t) &= -(n\hbar\omega-i\hbar\Gamma_1')(\rho_{22}-\rho_{23})^{n}(z,t) \\
&\quad+\frac{\mu_{\mathrm{ex}}}{2}\{E_p(z,t)[\rho_{12}^{n-1}(z,t)-\rho_{21}^{n-1}(z,t)]+E_p^*(z,t)[\rho_{12}^{n+1}(z,t)-\rho_{21}^{n+1}(z,t)]\} \\
&\quad-\mu_{\mathrm{bi}}\{E_p(z,t)[\rho_{23}^{n-1}(z,t)-\rho_{32}^{n-1}(z,t)]+E_p^*(z,t)[\rho_{23}^{n+1}(z,t)-\rho_{32}^{n+1}(z,t)]\} .
\end{aligned}
\tag{28}
$$

Equations (28) form an infinite set of simultaneous differential equations which can be truncated to $|n|\leq 2$. It was shown[9,11] that if one considers the functions $(\rho_{11}-\rho_{22})^0(z,t)$, $(\rho_{22}-\rho_{33})^0(z,t)$, $\rho_{12}^1(z,t)$, $\rho_{21}^1(z,t)$, $\rho_{13}^2(z,t)$, $\rho_{31}^2(z,t)$, $\rho_{23}^1(z,t)$, and $\rho_{32}^1(z,t)$ together with their complex conjugates, the dielectric function in the steady-state regime can be described within a very good approximation. The system is then reduced to 14 coupled differential equations which can be solved numerically to get the susceptibility [Eq. (26)].

To calculate the susceptibility, we need to obtain the coherent and incoherent parts separately. In order to do this, let us go back to Eq. (27), which represents the time evolution of the density matrix. If we now build up an ensemble average over the quasiparticle population, then Γ_{ii} represents the energy transfer from the exciton-biexciton system towards a heat bath, $T_i=1/\Gamma_{ii}$ being the corresponding decay time due to inelastic collisions. These dampings do not give information on the time evolution of the actual states which are excited coherently. If we now calculate the susceptibility using these dampings together with the Γ_{ij} which corresponds to the phase relaxation of the quasiparticle states, then we get both the coherent and the incoherent parts of the nonlinear susceptibility $\chi_{\mathrm{NL}}(z,t)$.

In the case of direct-band-gap semiconductors, Γ_{ii} is of the order of ns^{-1} and Γ_{ij} of ps^{-1}. In order to separate the two parts of the susceptibility, we build an ensemble average, made of equivalent states. Then, Eq. (27) represents the time evolution of the states which are excited coherently. We denote their decay time by τ_i. They are limited by both elastic and inelastic collision

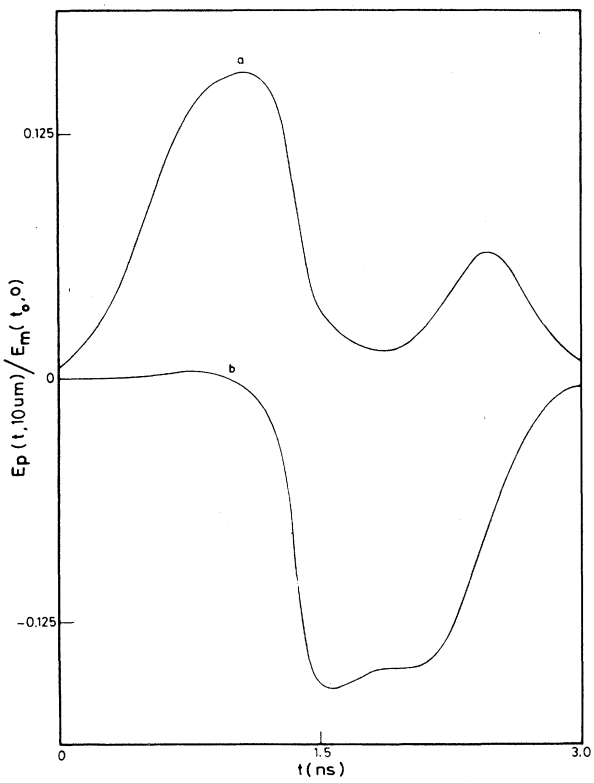

FIG. 3. Time dependence of the real (curve *a*) and imaginary (curve *b*) parts of the electric field amplitude of the pump pulse relative to its maximum incident amplitude $[(n_p)^{1/2}]$ after its propagation through the sample for the conditions of curve *a* of Fig. 1.

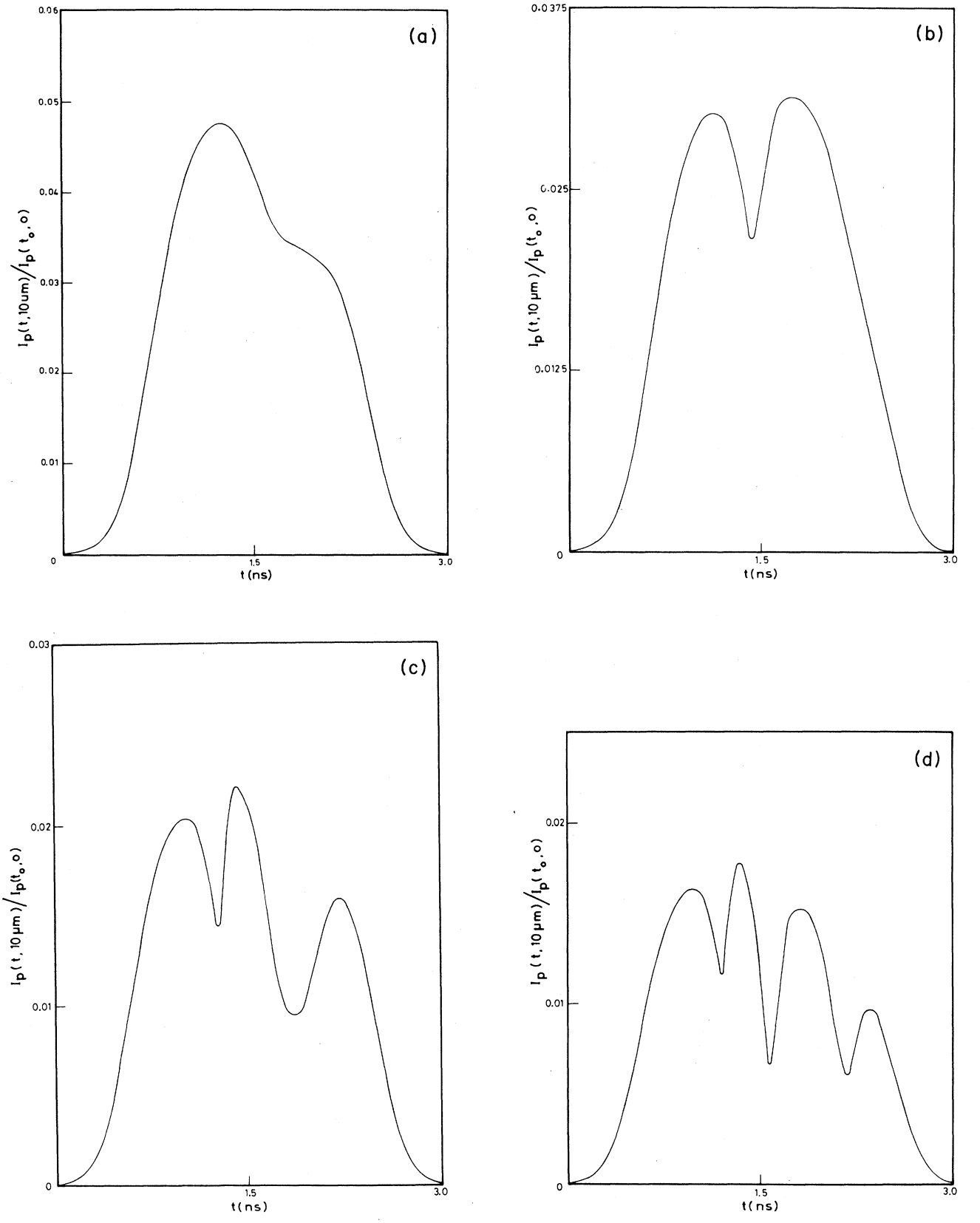

FIG. 4. Same as curve *a* of Fig. 1, but for different maximum intensities of the incident pump pulse, n_p having the following values (in photons/cm^3): (a) 2.5×10^{14}, (b) 4×10^{14}, (c) 5×10^{14}, and (d) 7.5×10^{14}.

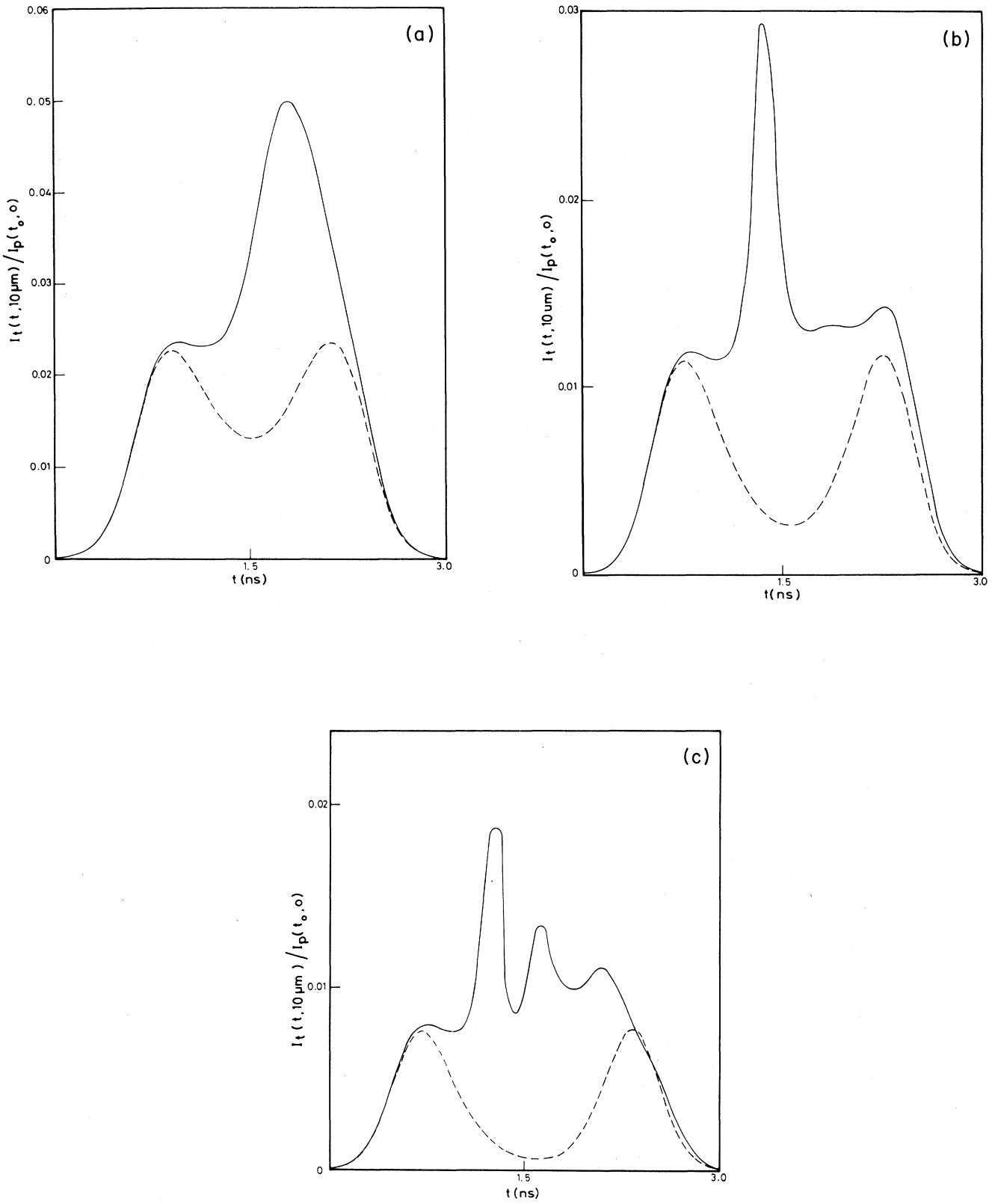

FIG. 5. Temporal shape of the test pulse when taking into account its propagation through the sample compared to the shape obtained within the mean-field approximation (the dotted line) for different maximum input pulse intensities, n_p having the values (in photons/cm^3) (a) 2.5×10^{14}, (b) 5×10^{14}, and (c) 7.5×10^{14}.

processes. Considering quasistationary states,[22] these lifetimes give rise to the nondiagonal damping constant of the density matrix through

$$\Gamma_{ij}=\frac{1}{2}\left[\frac{1}{\tau_i}+\frac{1}{\tau_j}\right] . \tag{29}$$

If we now calculate the susceptibility using $1/\tau_i$ as diagonal damping constants, we only get the coherent contribution of the susceptibility, which we will call $\chi_{\rm co}$. Then Eq. (25) is reduced to

$$E_p^*(z,t)\chi_{\rm NL}^{(2)*}(z,t)=E_p[\chi_{\rm co}(z,t)-\chi_L] . \tag{30}$$

Using, now Eqs. (29) and (30) we can get $\chi_{\rm NL}^{(0)}(z,t)$ and $\chi_{\rm NL}^{(2)*}(z,t)$ and the incoherent susceptibility part through

$$\chi_{\rm in}=\chi-\chi_{\rm co} .$$

As we have seen, the pump field can be calculated from Eq. (14) as a function of A and B which in turn, are functions of the pump field through the rate equations. Some kind of iteration now has to be performed. To do this, we follow the procedure mentioned in Sec. I. Namely, we treat the problem as if the sample was cut into slices. For the first slice, the input pump and test fields [$E_p^{(1)}(z,t)$ and $E_t^{(1)}(z,t)$ in Eq. (14)] are taken as Gaussian pulses of the form

$$E(0,t)=(I_0+I_m e^{-[(t-t_0)/\tau]^2})^{1/2} . \tag{31}$$

For computational reasons, I_0 has to be chosen different from zero. τ is the width of the pulse. The value of t_0 is chosen to be equal to 3τ and the integration of Eq. (27) is performed in the range from 0 to 6τ. In the present case, dealing with ns pulses, we have chosen $\tau=500$ ps. For the first interval of the time integration, we took for the mean field the value

$$E_p^m=\left[\frac{I_0}{2\alpha_L\Delta z}(1-e^{-2\alpha_L\Delta z})\right]^{1/2} ,$$

where α_L is the linear absorption coefficient. For the other time intervals or for the other slices, we use Eq. (16) for the mean field and then obtain the susceptibility. We use Eq. (14) to get the fields. For all the parameters we took the same values as in Ref. 8, except for the Γ's, where we used the values $\hbar/2\tau_2=\hbar/2\tau_3=10^{-4}$ eV, $\hbar\Gamma_{ii}=10^{-6}$ eV, and $\hbar/\tau_1=0$.

III. THEORETICAL RESULTS AND DISCUSSION

A. Pulse shapes after propagation through samples of 10 μm thickness

Let us first consider the propagation of the pump pulse through a sample of 10 μm thickness. The maximum incident intensity is chosen to be 3 MW/cm^2 which corresponds to a photon density of approximately $n_p=5\times10^{14}$ cm^{-3} in CuCl. The excitation frequency is at $\hbar\omega_p=3.186$ eV, i.e., at the biexciton two-photon resonance. Figure 1(a) shows the temporal shape of the initially Gaussian pulse when transmitted through the sample as calculated from Eq. (16), using 69 slices of variable thickness. Compared to Fig. 1(b) when the source term $\chi_{\rm NL}^{(2)*}$ has been neglected, the pulse becomes quite structured and its intensity is increased at the end of the pulse due to the induced recombination of the biexcitons. Figures 1(c) and 1(d) give the same information when the mean-field approximation is applied. In this approximation, all spatial variations are neglected and the field is assumed to be constant throughout the sample. The pulse intensities then obtained are much higher and the structures which remain are only due to the temporal variation of α and λ^2. As we see from Fig. 1, the mean-field approximation gives, qualitatively and quantitatively, results different from the pulse propagation under these excitation conditions. In addition, the pulse becomes much more structured if the regeneration term and the propagation are properly included, and these structures show up at much lower intensities than in the mean-field approximation. As shown in Fig. 2(a), the absorption approximately follows the pump-pulse intensity without affecting its shape considerably. As we will see later on, α influences the pulse shape only at the beginning of the propagation (in about the first micrometer). However, it is mainly responsible for the regeneration of the pulse, and thus the signal generation has a different shape. It gives rise to gain ($\lambda^2>0$) at the beginning of the pulse and to attenuated oscillation ($\lambda^2<0$) at its end. The fact that structures appear in the pulse shape is due to the effect of gain and attenuated oscillation of the pump field as well as to its phase change, induced by the propagation. This is clearly shown in Fig. 3, where we have plotted the real

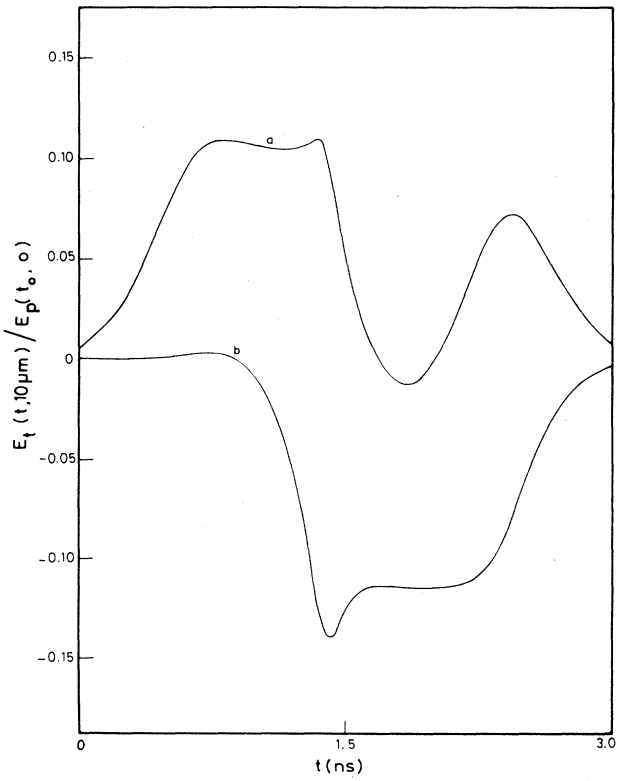

FIG. 6. Same as Fig. 3, but for the test field.

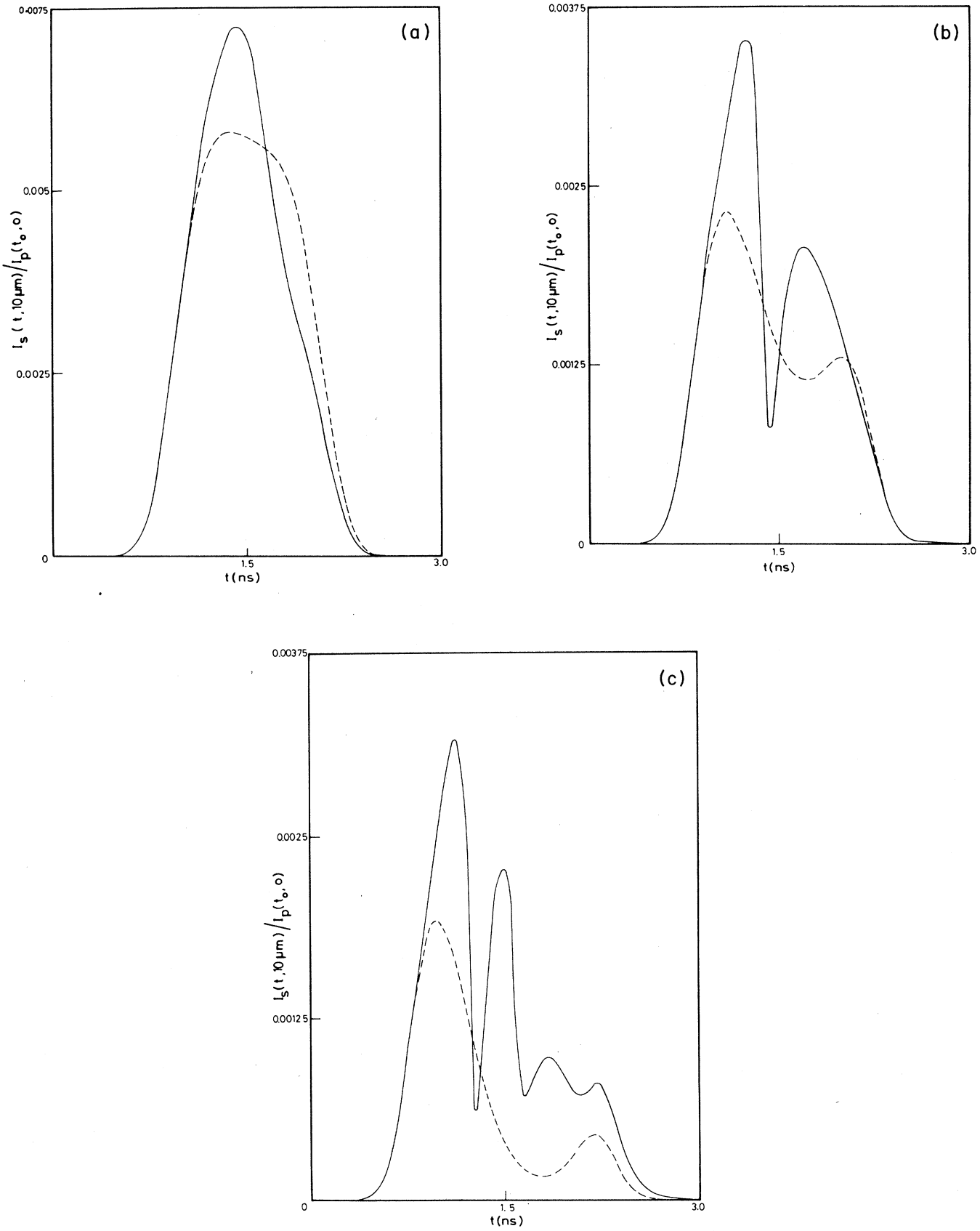

FIG. 7. Same as Fig. 5, but for the generated signal-pulse intensities.

and imaginary parts of the field at the end of the sample. It is worth remembering that the incoming fields have a Gaussian shape and are real. The imaginary part of the field is generated through the propagation only. This can be understood if we look at the real E_{p_1} and imaginary E_{p_2} parts of Eq. (14) for the case of the pump field separately, which corresponds to a system of coupled equations:

$$E_{p_1}=e^{a_1 z}\left[E_{p_1}^{(1)}\left[\cosh\lambda z+b_1\frac{\sinh\lambda z}{\lambda}\right]-E_{p_2}^{(1)}(a_2-b_2)\frac{\sinh\lambda z}{\lambda}\right],$$

$$E_{p_2}=e^{a_1 z}\left[E_{p_2}^{(1)}\left[\cosh\lambda z-b_1\frac{\sinh\lambda z}{\lambda}\right]+E_{p_1}^{(1)}(a_2+b_2)\frac{\sinh\lambda t}{\lambda}\right],$$

respectively. In Fig. 4, we show how these structures develop with increasing intensity. As already stated in Ref. 9 for the stationary case, at even higher maximum intensities than $n_p=10^{15}$ cm^{-3}, the system becomes unstable and no correct pulse shape can be established, at least for the damping constants used here.

Since, in the pump pulse, strong temporal structures are generated through the propagation, these structures show up in the test and the signal pulse, as can be seen in Figs. 5–8. Figure 5 shows the test-pulse shape for different intensities up to $n_p=7.5\times10^{14}$ cm^{-3} as a function of time, and compared with the mean-field results. Figure 6 gives the real and imaginary parts of the test field for $n_p=5\times10^{14}$ cm^{-3}. It clearly shows the origin of the spike in the intensity around 1.4 ns. In this case, the real part of the field is still large and the imaginary part almost reaches its minimum value. Figures 7 and 8 show results similar to Figs. 5 and 6 for the generated signal. One should point out here that these differences between the mean-field theory and the propagation show up at high intensities and at the biexciton resonance. Outside the resonance, both theories give the same results since $\alpha l \ll 1$.

B. Propagation effects at fixed temporal positions in the pulse envelope

Besides the pulse shapes obtained after propagation through the sample, it is also interesting to study how the pulses evolve inside the samples. In order to discuss this point in more detail, we have first studied how λ^2 and α behave at a fixed time position ($t=1.5$ ns, i.e., at the maximum of the incoming pulse) inside the crystal. The result is shown in Fig. 9. Both λ^2 and α have very high values in the first micrometer and then reach their low-intensity values. This behavior explains why the shapes of the different pulses are practically established after a propagation through a slice of about $\lesssim 1$ μm. These tem-

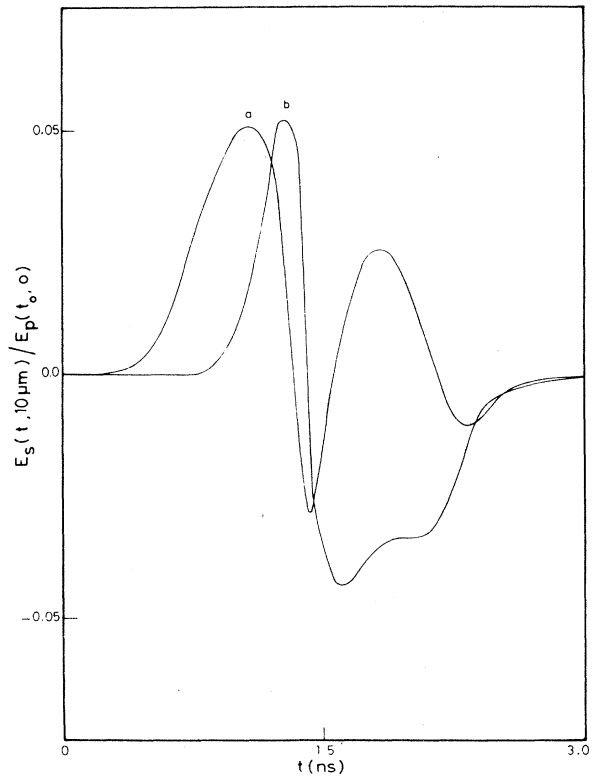

FIG. 8. Same as Fig. 3, but for the generated signal field.

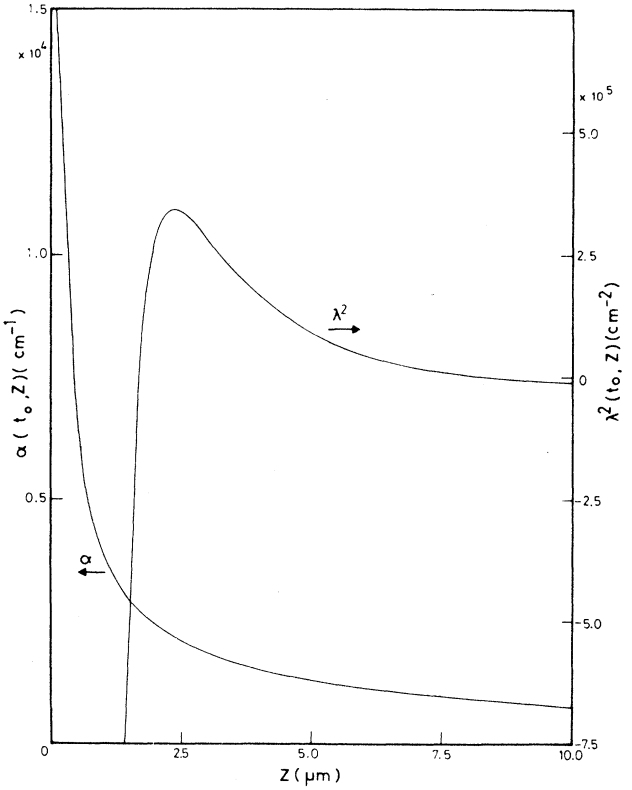

FIG. 9. Spatial evolution of the absorption coefficient α and the regeneration function χ^2 at a maximum incident pump-pulse intensity $n_p=5\times10^{14}$ photons/cm^3 for $t=t_0=1.5$ ns.

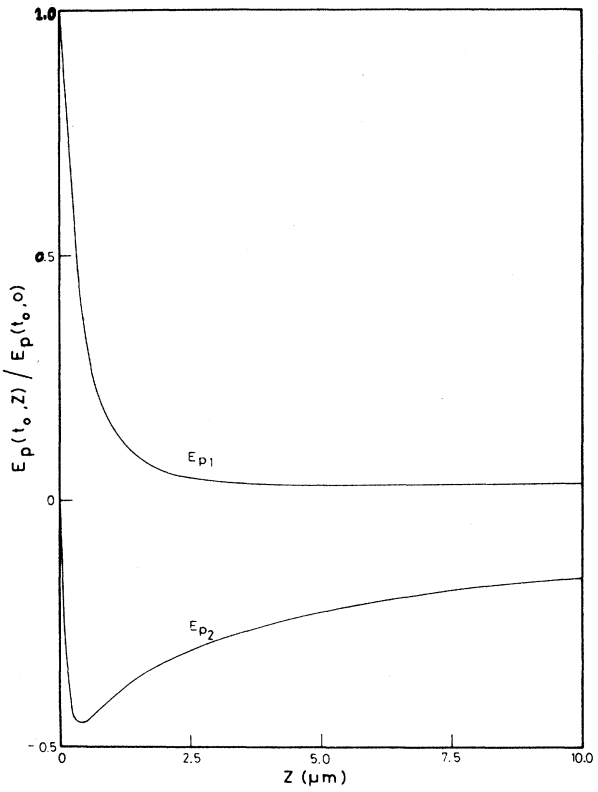

FIG. 10. Spatial evolution of the real and imaginary parts of the pump field relative to a maximum incident pump field $[(n_p)^{1/2}]$ at $n_p = 5\times 10^{14}$ photons/cm^3 at $t = t_0$.

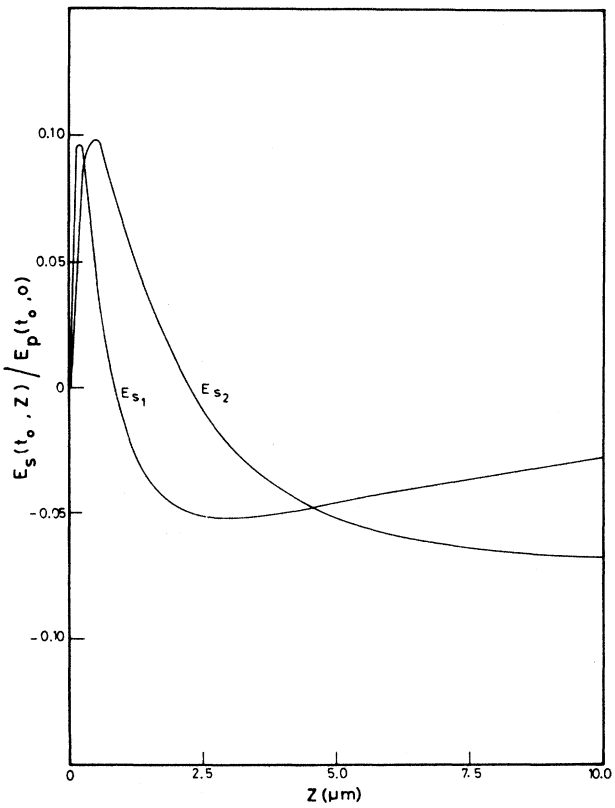

FIG. 11. Same as Fig. 10, but for the signal field.

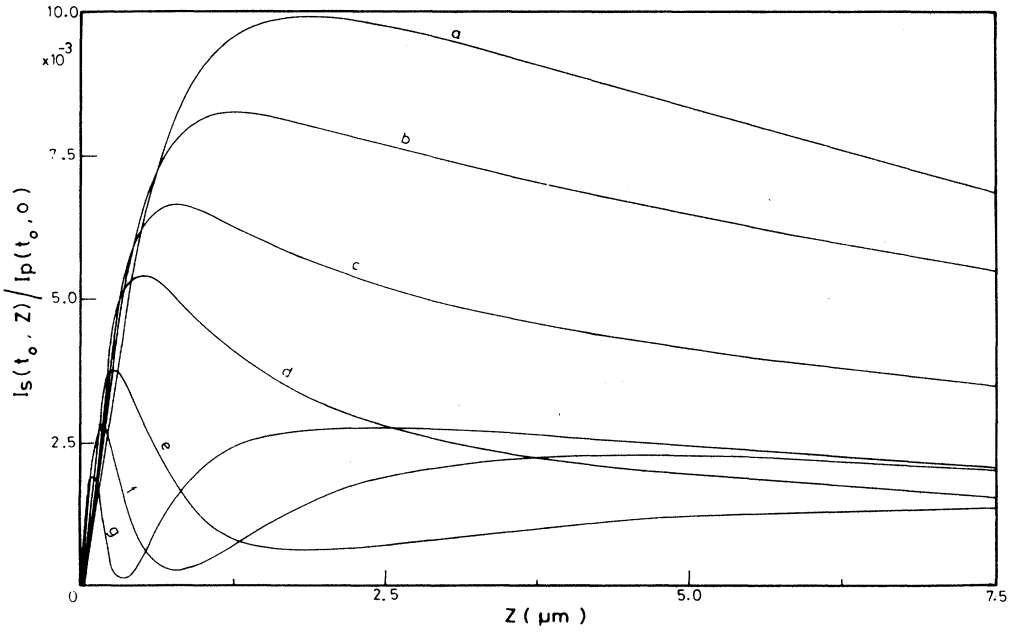

FIG. 12. Spatial evolution of the generated signal intensity at $t = t_0$ for different maximum intensities of the incident Gaussian pump pulse, when n_p has the values (in photons/cm^3) *a*, 2.5×10^{14}; *b*, 3×10^{14}; *c*, 3.5×10^{14}; *d*, 4×10^{14}; *e*, 5×10^{14}; *f*, 6×10^{14}; and *g*, 7.5×10^{14}.

poral shapes are maintained afterwards. In the case of the test pulse, only its overall intensity decreases due to absorption. In Fig. 10 we show the evolution of the pump fields for the real $[E_{p_1}(z,t_0)]$ and imaginary $[E_{p_2}(z,t_0)]$ parts corresponding to Fig. 9, and Fig. 11 that of the signal fields. Although the dephasing of the signal is important, its overall shape remains almost unchanged. Only the temporal positions of the relative maxima and minima of the pulse in Fig. 7 are slightly shifted. This is shown in Fig. 12, where for low intensities only one maximum appears, since the pulses do not present any structures, but do present a nearly Gaussian form. Then, at higher intensities, the structures appear first in the trailing edge of the pulse (as shown in Fig. 7) and then move with higher intensities towards the leading edge. This explains the relative maxima and minima of $I_s(z,t_0)$ at higher intensities. If one plots the absolute maximum of the generated pulse as a function of z, independently of its temporal position, curves like those at low intensities are obtained.

IV. CONCLUSION

We have shown that the propagation effects in a nonlinear medium modify the pulse shapes tremendously. These effects are important even at quite low intensities at resonance where one would expect the mean-field approximation to be valid. A great deal of these temporal and spatial structures are due to the dephasing between the real and imaginary parts of the fields, the last part being due to the generation process which results from the induced recombination. It gives rise to the signal generation as well as to an important reconstitution of the pump pulse. The different temporal behaviors of this coherent process (λ^2) with respect to the nonlinear absorption (α) have been completely neglected, to our knowledge, up to now.

ACKNOWLEDGMENTS

The authors are grateful to Dr. J. B. Grun, Dr. H. Haug, Dr. J. M. Hvam, Dr. C. Klingshirn, and Dr. R. Levy for many useful discussions on the signal-generation process. One of the authors (S.M.) would like to thank the French Mission of Research and Cooperation in Cairo and the Ministry of French Foreign Affairs for financial support. This work has been supported by a contract from the Formation des Ingenieurs par la Recherche Technologique (FIRTECH) program of the Ministère de la Recherche et de l'Enseignement Supérieur for Optics and Electro-optics of Orsay (France). It has been furthermore supported by an International Cooperation between the Centre National de la Recherche Scientifique (France) (CNRS) and the Conseil National de Recherches du Canada (Ottawa, Canada) (CNRC).

*On leave from Laboratory of Laser Physics and its Applications, Department of Physics, Faculty of Science, Cairo University, Cairo, Egypt.

†Permanent address: Department of Physics, Université du Québec à Trois-Rivières, C.P. 500, Trois-Rivières, Québec, Canada G9A 5H7.

[1]A. Maruani, J. L. Oudar, E. Batifol, and D. S. Chemla, Phys. Rev. Lett. **41**, 1372 (1978).

[2]D. S. Chemla, A. Maruani, and E. Batifol, Phys. Rev. Lett. **42**, 1075 (1978).

[3]L. Schultheis, J. Kuhl, A. Honold, and C. W. Tu, Phys. Rev. Lett. **57**, 1797 (1986).

[4]J. M. Hvam, I. Balslev, and B. Hönerlage, Europhys. Lett. **4**, 839 (1987).

[5]T. Yajima and Y. Taira, J. Phys. Soc. Jpn. **47**, 1620 (1979).

[6]G. Grynberg and M. Pinard, Phys. Rev. A **32**, 3772 (1985).

[7]J. W. Haus, C. M. Bowden, and C. C. Sung, Phys. Rev. A **31**, 1936 (1985).

[8]Vu Duy Phach, A. Bivas, B. Hönerlage, and J. B. Grun, Phys. Status Solidi B **84**, 731 (1977).

[9]B. Hönerlage and J. Y. Bigot, Phys. Status Solidi B **124**, 221 (1984).

[10]B. März, S. Schmitt-Rink, and H. Haug, Z. Phys. B **40**, 9 (1980).

[11]J. Y. Bigot, J. Miletic, and B. Hönerlage, Phys. Rev. B **32**, 6478 (1985).

[12]R. Levy, J. Y. Bigot, and B. Hönerlage, Solid State Commun. **61**, 331 (1987).

[13]R. Leonelli, J. C. Mathae, J. M. Hvam, and R. Levy, in *Proceedings of the 18th International Conference on the Physics of Semiconductors, Stockholm, Sweden,* edited by O. Engström (World Scientific, Singapore, 1986), p. 1437.

[14]M. Frindi, B. Hönerlage, and R. Levy, Phys. Status Solidi B **138**, 1437 (1986).

[15]B. Hönerlage and J. Miletic, Europhys. Lett. **7**, 19 (1988).

[16]B. Hönerlage, M. Frindi, and J. Miletic, Phys. Status Solidi B **149**, 382 (1988).

[17]J. Y. Bigot and B. Hönerlage, Phys. Rev. A **36**, 715 (1987).

[18]A. Maruani and D. S. Chemla, Phys. Rev. B **23**, 841 (1981).

[19]B. Hönerlage, R. Levy, J. B. Grun, C. Klingshirn, and K. Bohnert, Phys. Rep. **124**, 161 (1985).

[20]A. Yariv, *Quantum Electronics,* 2nd ed. (Wiley, New York, 1975).

[21]A. Schenzle, and R. G. Brewer, Phys. Rev. A **14**, 1756 (1976).

[22]A. S. Davydow, *Quantenmechanik* (Verlag der Wissenschaften, Berlin, 1967).